ELSEVIER

Microelectronics Journal 37 (2006) 1461–1467

Microelectronics Journal

www.elsevier.com/locate/mejo

Wavelength controlled InAs/InP quantum dots for telecom laser applications

S. Anantathanasarn*, R. Nötzel, P.J. van Veldhoven, F.W.M. van Otten, Y. Barbarin, G. Servanton, T. de Vries, E. Smalbrugge, E.J. Geluk, T.J. Eijkemans, E.A.J.M. Bente, Y.S. Oei, M.K. Smit, J.H. Wolter

eiTT/COBRA Inter-University Research Institute on Communication Technology, Eindhoven University of Technology, 5600 MB Eindhoven, The Netherlands

Available online 18 July 2006

Abstract

This article reviews the recent progress in the growth and device applications of InAs/InP quantum dots (QDs) for telecom applications. Wavelength tuning of the metalorganic vapor-phase epitaxy grown single layer and stacked InAs QDs embedded in InGaAsP/InP (1 0 0) over the 1.55-μm region at room temperature (RT) is achieved using ultra-thin GaAs interlayers underneath the QDs. The GaAs interlayers, together with reduced growth temperature and V/III ratio, and extended growth interruption suppress As/P exchange to reduce the QD height in a controlled way. Device quality of the QDs is demonstrated by temperature-dependent photoluminescence (PL) measurements, revealing zero-dimensional carrier confinement and defect-free InAs QDs, and is highlighted by continuous-wave ground-state lasing at RT of narrow ridge-waveguide QD lasers, exhibiting a broad gain spectrum. Unpolarized PL from the cleaved side, important for realization of polarization insensitive semiconductor optical amplifiers, is obtained from closely stacked QDs due to vertical electronic coupling.
© 2006 Elsevier Ltd. All rights reserved.

Keywords: InAs; InGaAsP; InP (1 0 0); Quantum dot; Metalorganic vapor-phase epitaxy; Laser

1. Introduction

Semiconductor quantum dots (QDs) enable superior performance of optical devices such as lasers and semiconductor optical amplifiers (SOAs) and are potential candidates for future solid-state quantum information and communication [1–3]. This is based on their discrete, atomic-like energy states, improving device parameters like threshold current, gain, temperature characteristics, and allowing the control of single photons and charge carriers. Being compatible with tomorrow's global information and communication infrastructure demands device operation in the 1.55 μm wavelength region, which is the minimum absorption window of glass fibers. Unfortunately, the optical quality of self-assembled InAs/GaAs QDs, most widely employed, strongly degrades for emission wavelengths larger than 1.3 μm.

This calls for the InAs/InP materials system which is ideally suited for 1.55 μm telecom optical devices. Controlling, however, the emission wavelength of self-assembled InAs/InP QDs in the 1.55-μm region is still a challenge. This is primarily due to the small lattice mismatch and the presence of As/P exchange during InAs growth on InP-based materials [4], resulting in relatively large QDs with emission wavelengths far beyond 1.6 μm at room temperature (RT). As/P exchange is anticipated to be most pronounced in metalorganic vapor-phase epitaxy (MOVPE) due to high growth temperature, high reactor pressure, long gas-phase diffusion, and complex gas exchange as compared to chemical beam epitaxy (CBE) and molecular beam epitaxy (MBE).

In this paper, we report the successful control of the emission wavelength and device applications of single layer and stacked InAs QDs embedded in a lattice-matched

*Corresponding author. Tel.: +31 40 247 8371; fax: +31 40 246 1339.
E-mail address: S.Anantathanasarn@tue.nl (S. Anantathanasarn).

0026-2692/$ - see front matter © 2006 Elsevier Ltd. All rights reserved.
doi:10.1016/j.mejo.2006.05.028

InGaAsP ($\lambda_Q = 1.25\,\mu m$; Q1.25) matrix on InP (1 0 0) by MOVPE. Once the basic growth conditions like temperature, gas switching sequence, and V/III ratio are set, insertion of ultrathin GaAs interlayers allows continuous tuning of the emission wavelength over the 1.55 μm region [5–7]. Zero-dimensional carrier confinement and defect-free InAs QDs are demonstrated by temperature-dependent photoluminescence (PL) measurements. Narrow ridge-waveguide QD lasers operate in continuous-wave (CW) mode at RT on the QD ground state transition and exhibit a broad gain spectrum. Linear polarization insensitive PL emission from the cleaved side, which is crucial for applicability of photonic devices in fiber-optical telecom systems, is achieved by close stacking of the QD layers.

2. Sample structure

The samples were grown on InP (1 0 0) substrates, misoriented 2° toward (1 1 0), by MOVPE using trimethyl-indium (TMI), trimethyl-gallium (TMG), tertiarybutyl-arsine (TBA), and tertiarybutyl-phosphine (TBP) as gas sources with hydrogen as carrier gas. The sample structure commenced with 100 nm InP followed by single or stacked InAs QDs plus GaAs interlayers underneath placed in the center of the lattice-matched Q1.25 layer with thickness of 200–500 nm, grown at 500 °C. The GaAs interlayer thickness (d_{GaAs}) was 0–2 monolayers (MLs), the nominal amount of InAs for QD formation was 3 and 3.5 MLs, and the Q1.25 separation layer thickness between the stacked QDs was 40 and 4 nm. On the sample surface the InAs QDs plus GaAs interlayer were repeated for atomic force microscopy (AFM). The optical properties were measured by PL spectroscopy using a Nd:YAG laser (532 nm) as excitation source with excitation power density of 256 mW/cm^2. The narrow ridge-waveguide Fabry-Pérot laser diodes contained a 500 nm Q1.25 waveguide core with 5-stacked InAs QD layers separated by 40 nm Q1.25 grown at 500 °C. The 500 nm n-InP bottom cladding on n-InP substrate and the 1.5 μm p-InP top cladding, completed by a compositionally graded 75-nm p-InGaAsP contact layer, were grown at 585 °C. The width of the ridge waveguide, defined by optical lithography and reactive ion etching was 3.5 μm and the cleaved cavity was between 1 and 3.6 mm long.

It is important to note that our device structure is compatible with photonic integration, combining active and passive devices on a single chip. The Q1.25 layer forming the waveguide core compromises maximum confinement energy of the QDs (small λ_Q) in active devices with a large electro-optic effect (large λ_Q) for phase modulation. Moreover, a large λ_Q enhances the refractive index contrast with respect to the waveguide cladding for strong optical mode confinement in compact devices. Reports on InAs/InP QD lasers so far have employed larger bandgap Q waveguide cores or even Al-containing material [8–12], which is not preferred due to surface contamination and polycrystalline deposition on dielectric masked areas hindering defect-free selective active–passive re-growth. Growth is performed by MOVPE on InP (1 0 0) substrates to comply with production standards.

3. Emission wavelength controlled QDs

3.1. Suppression of As/P exchange reaction

The morphology of the InAs QDs is round and dome-shaped, similar to that obtained by CBE [5], with a QD density of $\sim 3 \times 10^{10}\,cm^{-2}$. The PL peak emission wavelength of the QDs (λ_{QD}), however, is beyond 1600 nm even at 4.8 K, as shown in Fig. 1(a). The PL spectra at 4.8 K of the InAs QDs with 2 MLs GaAs interlayer without and with an additional flushing step under various TBA flows are depicted in Fig. 1(b–d). The average QD height (h_{QD}) in the presence of the GaAs interlayer is reduced from 6.0 to 3.1 nm and λ_{QD} is blue-shifted to 1580 nm confirming suppressed As/P exchange. This is understood by compar-

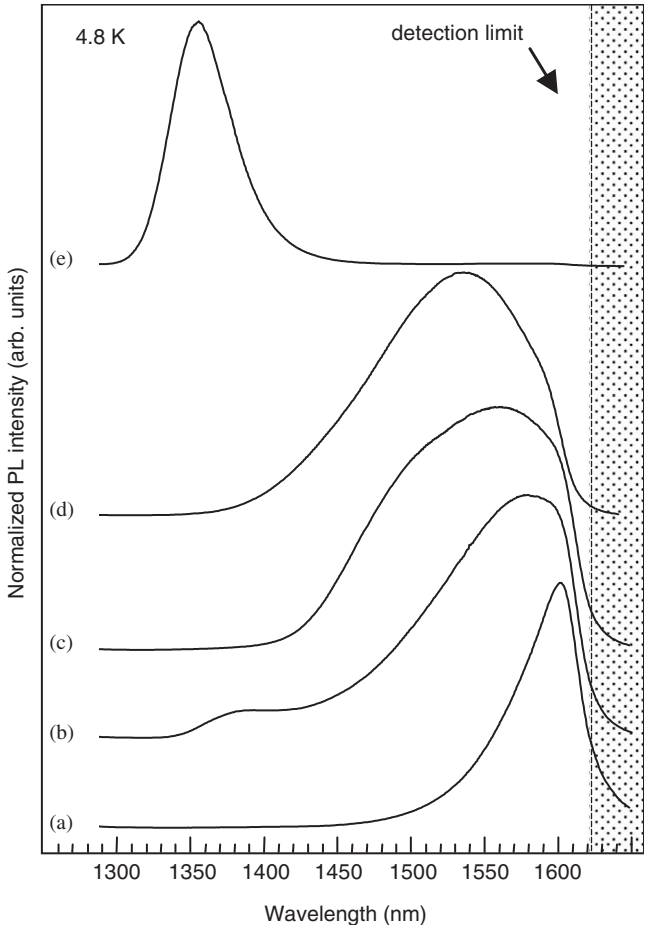

Fig. 1. Normalized PL spectra taken at 4.8 K of the 3 MLs InAs single QD layers grown (a) without and (b) with 2 MLs GaAs interlayer at a TBA flow rate of 6.1 sccm. (c–e) PL spectra of the QDs with 2 MLs GaAs interlayer and TMG flushing grown at a TBA flow rate of (c) 6.1, (d) 2.0, and (e) 1.0 sccm. The shaded area is above the detection limit of the cooled InGaAs detector at 1.6 μm.

ing the binary compound bond strengths. The In-As bond (bond enthalpy 48.0 kcal/mol) is more stable than the In-P bond (47.3 kcal/mol). On the other hand, both the Ga–As (50.1 kcal/mol) and Ga–P (54.9 kcal/mol) bonds are more stable than the In–As and In–P bonds. Hence, GaAs surface passivation prevents the replacement of P bound to In by As.

The shoulder observed on the short-wavelength side of the PL spectrum in Fig. 1(b) is attributed to inhomogeneous Ga incorporation in the QD layer caused by residual TMG in the reactor. Optimized gas switching with a TMG flushing step for 45 s under TBA flow after GaAs interlayer growth ensures pure TMI as group-III source for QD formation. This realizes uniform InAs QDs with smaller QD size, no shoulder in the PL spectrum, and an additional blue-shift to 1558 nm as shown in Fig. 1(c).

The effect of the V/III ratio on InAs QD formation is studied by reducing the TBA flow rate from 6.1 sccm (TBA partial pressure (p_p) = 0.0059 mbar) in the previous experiments to 2.0 sccm (p_p = 0.0019 mbar) and 1.0 sccm (p_p = 0.0009 mbar), while keeping the TMI flow rate constant. These TBA flow rates correspond to V/III ratios of 1.26, 0.4, and 0.2, determined from the corresponding TBA and TMI partial pressures. For 6.1 sccm TBA flow rate, λ_{QD} is 1558 nm at 4.8 K and beyond 1600 nm at RT despite of the small QD sizes. With reduction of the TBA flow, λ_{QD} continuously shifts to shorter wavelengths, reaching 1355 nm for the TBA flow rate of 1.0 sccm (Fig. 1(e)). Simultaneously, the PL linewidth becomes smaller, pointing toward reduced As/P exchange under low TBA flow, decreasing QD size fluctuations.

3.2. Wavelength control by GaAs interlayer thickness

After establishing the basic growth conditions such as temperature, gas switching sequence, and V/III ratio, the QDs emit at 1480 nm at RT in the presence of the 2 MLs GaAs interlayer. The QD emission is then tuned over the 1.55-μm wavelength region by reducing d_{GaAs}. As shown in Fig. 2(a), when d_{GaAs} is decreased to 1.2 MLs, λ_{QD} continuously shifts to 1560 nm (open squares). Simultaneously, the PL efficiency improves, which is attributed to the reduction of tensile strain for thinner d_{GaAs}, improving the structural quality. The average h_{QD} increases from 4.5 nm for 2 MLs GaAs to 5.6 nm for 1.2 MLs GaAs (Fig. 2(b)). The linear dependence of λ_{QD} on the GaAs interlayer thickness confirms the continuous suppression of As/P exchange to control the QD height and emission wavelength. Note that the slope of the linear dependence of λ_{QD} versus d_{GaAs} for the MOVPE-grown QD samples is steeper than that for the CBE grown ones (open triangles), indicating that InAs QD growth is more severely affected in MOVPE by the enhanced As/P exchange reaction.

Further reduction of d_{GaAs} into the submonolayer regime surprisingly shortens λ_{QD}. This is understood by the gradual shape transition from QDs to quantum dashes elongated along [0 $\bar{1}$ 1] for $d_{GaAs} < 1$ ML, as shown

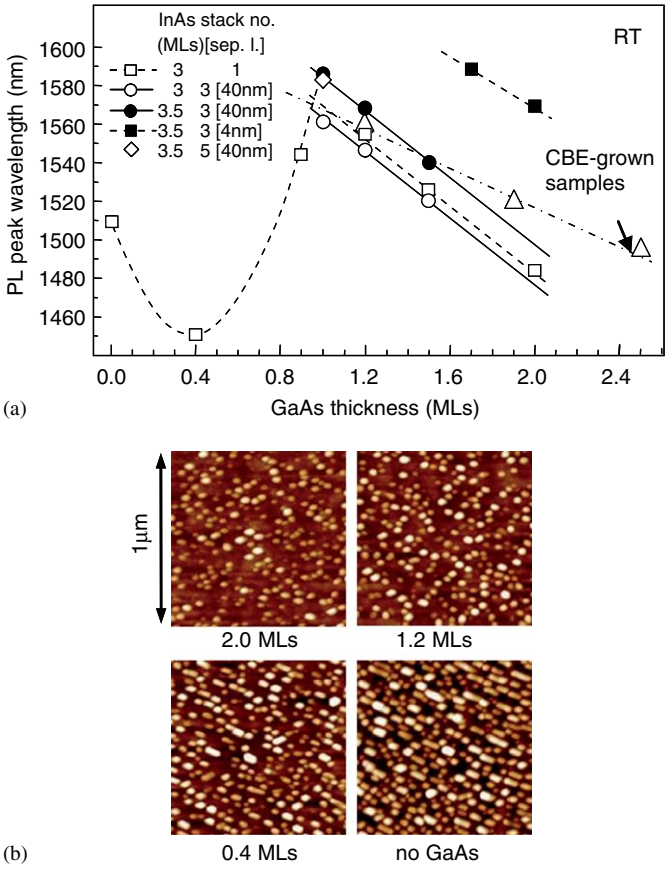

Fig. 2. PL peak wavelength at RT as a function of the GaAs interlayer thickness of the MOVPE-grown QD samples with various InAs amount, InGaAsP separation layer thickness, and number of stacked QD layers. Data from the CBE-grown samples (Ref. [5]) are shown for comparison. (b) AFM images of the 3 MLs InAs surface QDs with different GaAs interlayer thickness. The height contrast is 10 nm.

in Fig. 2(b). Evidently, the low TBA flow causes anisotropic In migration on the InGaAsP surface leading to dash formation and, moreover, favors P incorporation into the quantum dashes, causing the PL blue-shift. The minimum of λ_{QD} around d_{GaAs} = 0.4 MLs is attributed to the interplay between shape transition, shortening λ_{QD}, and As/P exchange, increasing the quantum dash height and PL emission wavelength. Only the combination of low growth temperature and low V/III ratio with the insertion of GaAs interlayers above one ML thickness allows continuous tuning of λ_{QD} over the 1.55 μm region without formation of dashes.

In order to increase the active volume, crucial for practical devices, the InAs QDs are stacked in up to 5 layers with 40 nm Q1.25 separation layers. λ_{QD} at RT of these widely-stacked QD samples shown in Fig. 2(a) is consistently reduced for increasing GaAs interlayer thickness due to the reduced QD height. The GaAs interlayer thickness is kept above one ML to avoid the formation of quantum dashes. The linear dependence of λ_{QD} for the 3-stacked 3 MLs InAs QDs on the GaAs interlayer thickness (open circles) almost coincides with that of the

single QD layers. The PL linewidths of the single and stacked QD layers are similar. Increasing the InAs amount of the 3-stacked QDs to 3.5 MLs shifts λ_{QD} by about 20 nm to larger values (solid circles) due to the larger QD height. The wavelength tuning with GaAs interlayer thickness remains unchanged, identifying the InAs amount together with the V/III ratio as other parameters to adjust the QD emission wavelength in combination with the GaAs interlayer, providing the highest PL efficiency slightly above one ML thickness. λ_{QD} of the 5-stacked 3.5 MLs InAs QDs lies on the same line (open diamond).

3.3. Optical properties

Detailed temperature dependent PL measurements between 4.8 K and RT of the 3-widely stacked 3.5 MLs InAs QDs with 1.5 MLs GaAs interlayer, emitting at 1540 nm at RT, are summarized in Fig. 3. The behavior of both the PL peak energy and linewidth shown in Fig. 3(a) is similar to that of InAs/GaAs QDs [13] and of the CBE-grown InAs/InGaAsP/InP QDs [14], originating from the zero-dimensional carrier confinement in inhomogeneous QD ensembles. The PL linewidth undergoes a minimum around 80–100 K due to thermally activated carrier redistribution, preferentially from smaller to larger QDs which is followed by equilibration of the carrier distribution at higher temperatures when thermally activated carrier escape from smaller and larger QDs becomes comparable. In the same temperature range, the PL peak energy reveals a steeper low-energy shift than the band gap calculated by the empirical Varshni law for InAs, confirming the preferential carrier occupation of larger QDs with lower energy.

The integrated QD PL intensity shown in Fig. 3(b) is almost constant at low temperature, undergoes a small maximum around 100 K due to carrier delocalization in the Q1.25 barrier layer, and exponentially decreases above 130–140 K. The activation energy (E_a) describing the quenching of the PL intensity is derived from a fit to [15]:

$$I_{PL} = \frac{C}{1 + A e^{-E_a/k_B T}}, \quad (1)$$

where k_B is the Boltzmann constant and T the temperature. C and A are fitting parameters. E_a amounts to 160 meV, which is close to the difference of the Q1.25 band gap and the InAs QD emission energy. Hence, the almost constant integrated PL intensity up to 140 K where substantial carrier redistribution takes place and the subsequent PL intensity quenching which is consistent with thermionic emission of carriers from the InAs QDs into the Q1.25 barriers confirm the excellent optical quality of the QDs, being free of non-radiative recombination centers. The PL efficiency at RT of the 3-stacked QDs is two orders of magnitude larger than that of the single QD layers. These results reveal identical reproduction and wavelength tuning of the InAs QDs upon wide stacking where vertical strain and electronic coupling can be neglected to increase the active volume without structural degradation.

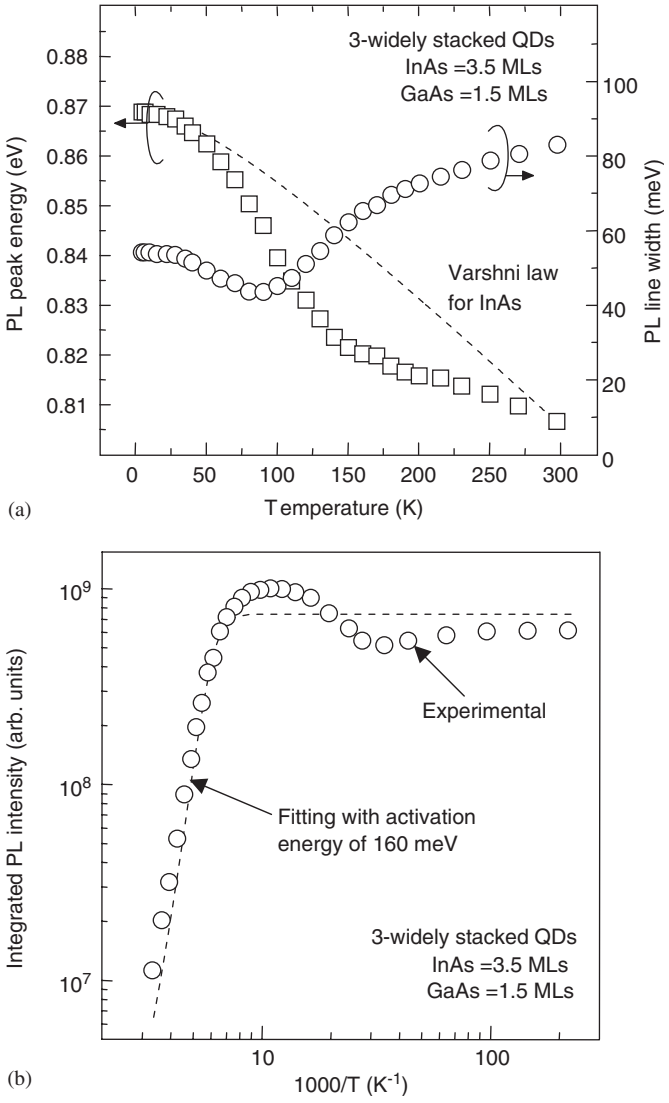

Fig. 3. (a) Temperature dependence of the PL peak energy and PL linewidth of the 3-widely stacked 3.5 MLs InAs QDs with 1.5 MLs GaAs interlayers. The dashed line is the temperature dependence of the InAs band gap energy according to the Varshni law. (b) Integrated PL intensity of the InAs QDs as a function of temperature. The dashed line is the exponential fit with thermal activation energy of 160 meV.

4. QD devices for telecom applications

4.1. QD laser

The cross-sectional scanning electron microscopy (SEM) image of the narrow ridge-waveguide laser, planarized by polyimide is shown in Fig. 4(a). The peak wavelength at RT of the PL of the 5-widely stacked InAs QDs taken from the surface after removal of the upper cladding is 1.58 μm and the PL linewidth is 110 meV. The electroluminescence (EL) and lasing spectra taken from the as-cleaved facet of the QD lasers with 1 and 3.6 mm cavity length are shown in

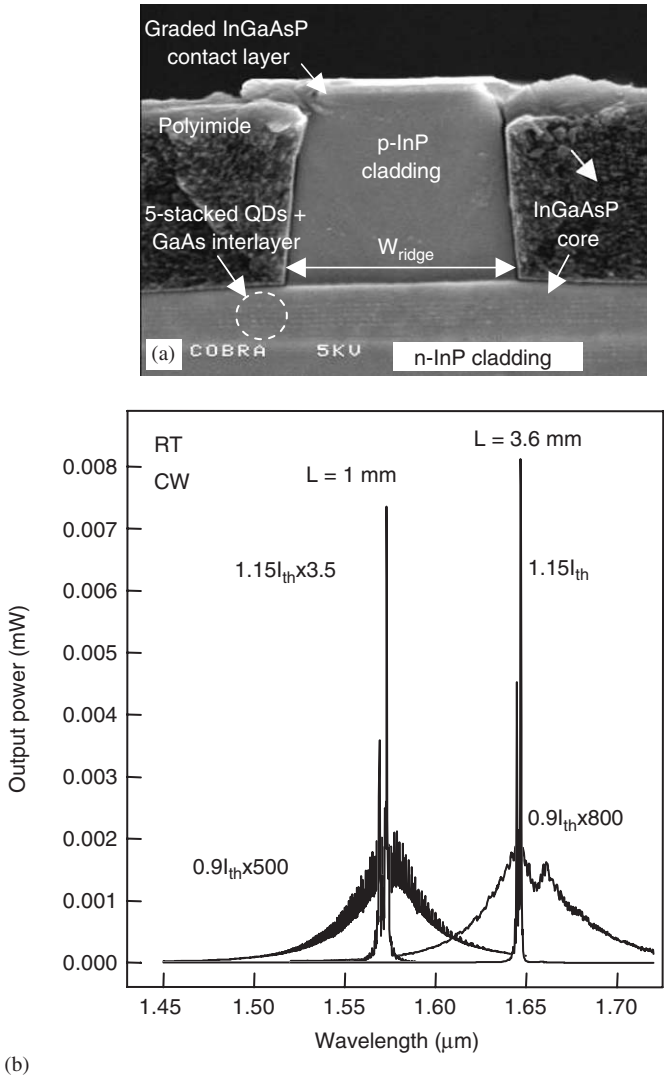

Fig. 4. (a) Cross-sectional SEM image of the QD laser structure. (b) EL and lasing spectra taken in CW mode at RT of the narrow ridge-waveguide QD lasers with cavity length, L, of 1 and 3.6 mm. The ridge width is 3.5 μm.

Fig. 4(b). Lasing near 1.55 μm in CW mode at RT on the QD ground state transition is successfully obtained for the 1-mm long device. Excited state lasing occurs at higher currents. The threshold current (I_{th}) is 125 mA, corresponding to a threshold current density (J_{th}) of 3.6 kA/cm^2. J_{th} is reduced to 1 kA/cm^2 for 3.6 mm device length owing to lower relative mirror loss, and the lasing wavelength is increased to 1.65 μm. This red-shift of the lasing wavelength is attributed to the fact that for longer devices already the QDs with lower density, having larger size within the distribution, are sufficient to overcome the cavity loss and support lasing [16].

When measuring in pulsed mode (165 ns pulse width and 300 kHz repetition rate), the threshold current is reduced to 74–78 mA due to suppressed heating. The linear relationship of J_{th} versus the inverse cavity length yields the transparency current density of 30 A/cm^2, i.e., 6 A/cm^2 per QD layer. The internal optical loss of 4.2 cm^{-1} and the internal differential quantum efficiency of 37% are deduced from the light output power versus current characteristics. The maximum achievable QD ground state modal gain is estimated to be 14.7 cm^{-1} from the 1-mm long device which is the shortest one lasing on the ground state transition. These values are among the best achieved [10–12], indicating the excellent quality and performance of our QDs despite of the lower confinement energy and QD density.

4.2. Towards QD SOAs

The QD gain spectrum, important for broadband SOAs and widely tunable lasers is determined from the Fabry-Pérot resonances in the CW amplified spontaneous emission (ASE) spectra below threshold [17] of the 1-mm long device using an ultra high-resolution (20 MHz) optical spectrum analyzer. The net modal gain, which includes the internal loss, as a function of wavelength for different currents is shown in Fig. 5. The gain peak wavelength blue-shifts with increasing current, revealing enhanced filling of smaller (shorter λ_{QD}) QDs. The maximum achievable QD ground state net modal gain is 10 cm^{-1} at 3.5 kA/cm^2 current density, taking into account that shorter devices lase on the excited state transition. The bandwidth of the gain spectrum at 3 dB amplification, determined from a parabolic fit, is 80 nm for the 1-mm long device.

Detrimental for applications in fiber-optical telecom systems is the transverse electric (TE) -polarized gain of QD SOAs regardless of the materials system and wavelength. This is due to the flat shape, i.e., shape anisotropy of the QDs, aligning the k-vectors of electrons and holes in-plane. As an important step towards polarization insensitive SOAs we demonstrate unpolarized PL emission from the cleaved side of closely stacked QDs due to vertical electronic coupling. λ_{QD} of the 3-closely stacked InAs QDs with 4 nm Q1.25 separation layers, depicted by solid

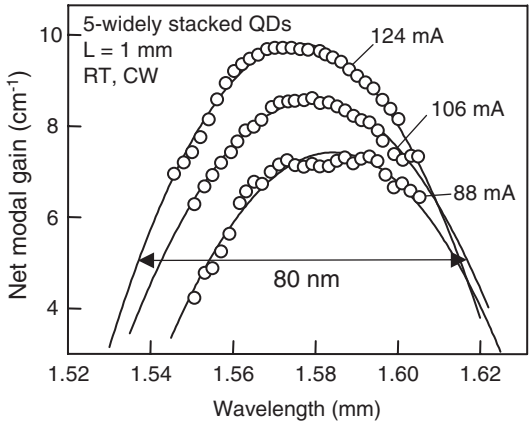

Fig. 5. Net modal gain versus wavelength for different currents (open circles) determined from the sub-threshold ASE spectra taken in CW mode at RT. The device length is 1 mm. The solid lines are parabolic fits.

squares in Fig. 2(a), is red-shifted by 90 nm with respect to that of the widely stacked QDs. Tuning of λ_{QD} with d_{GaAs} is unaltered. The PL linewidth at 4.8 K is reduced by more than 30 meV. Such PL red-shift and linewidth reduction indicates efficient electronic coupling in vertically aligned QDs, which is proven by the linear polarization of the cleaved-side PL in comparison to that of the widely stacked QDs.

The PL of the 3-widely stacked QDs, shown in Fig. 6(a), is TE polarized (in-plane) with a degree of linear polarization $P = (I_{TE}–I_{TM})/(I_{TE}+I_{TM})$ at the PL peak position of 0.7. In contrast, P for the 3-closely stacked QDs at the PL peak position is reduced to 0.1 and it crosses zero around 1.55 μm (Fig. 6(b)). Hence, the shape anisotropy of the closely stacked QDs is effectively reduced due to strong vertical electronic coupling to render the linear polarization of the cleaved-side PL from in-plane to isotropic. The PL efficiency of the 3-closely stacked QDs at RT is one order of magnitude larger than that of the single QD layer, confirming the good structural and optical quality of the QDs.

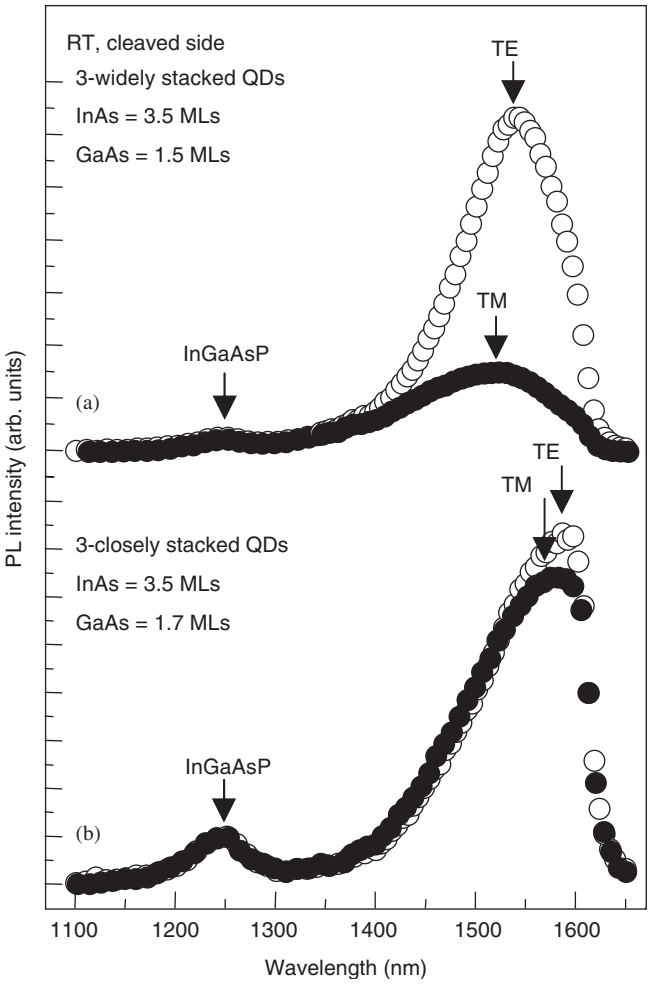

Fig. 6. Linear polarized PL spectra at RT taken from the cleaved side of the 3-stacked 3.5 MLs InAs QDs with InGaAsP separation layer thickness of (a) 40 nm and (b) 4 nm. The GaAs interlayer thickness is (a) 1.5 MLs and (b) 1.7 MLs. The detection limit of the cooled InGaAs detector is at 1600 nm.

5. Summary

In this article, the progress in realizing wavelength-controlled InAs/InP (1 0 0) QDs grown by MOVPE for telecom applications was overviewed. Wavelength tuning of single layer and stacked InAs QDs embedded in InGaAsP/InP (1 0 0) over the 1.55-μm region was achieved using ultrathin GaAs interlayers underneath the QDs. The GaAs interlayers, together with reduced growth temperature and V/III ratio, and extended growth interruption, suppress As/P exchange to reduce the QD height in a controlled way. Temperature-dependent PL measurements revealed zero-dimensional carrier confinement and defect-free InAs QDs. Ground-state lasing in CW mode at RT was achieved from narrow ridge-waveguide QD lasers, exhibiting a broad gain spectrum. Unpolarized PL from the cleaved side was obtained from closely stacked QDs due to vertical electronic coupling, which is crucial for the realization of polarization insensitive semiconductor optical amplifiers. Hence, wavelength tuning, lasing, and polarization control prove these QDs excellent for devices in fiber-optical telecom systems. Addressing the scope of this workshop we believe that exploration of nanostructure formation on high-index surfaces is of the highest importance if qualitatively new phenomena emerge [18–20]. Where possible, (1 0 0) is the surface orientation of choice.

Acknowledgements

This work is partially supported by ePIXnet (EU) and BBP Freeband (STW).

References

[1] Y. Arakawa, H. Sakaki, Appl. Phys. Lett. 40 (1982) 939.
[2] M. Asada, Y. Miyamoto, Y. Suematsu, IEEE J. Quantum Electron. QE-22 (1986) 1915.
[3] D. Loss, D.P. DiVincenzo, Phys. Rev. A 57 (1998) 120.
[4] S. Yoon, Y. Moon, T.-W. Lee, E. Yoon, Y.D. Kim, Appl. Phys. Lett. 74 (1999) 2029.
[5] Q. Gong, R. Nötzel, P.J. van Veldhoven, T.J. Eijkemans, J.H. Wolter, Appl. Phys. Lett. 84 (2004) 275.
[6] S. Anantathanasarn, R. Nötzel, P.J. van Veldhoven, T.J. Eijkemans, J.H. Wolter, J. Appl. Phys. 98 (2005) 013503.
[7] S. Anantathanasarn, R. Nötzel, P.J. van Veldhoven, F.W.M. van Otten, T.J. Eijkemans, J.H. Wolter, Appl. Phys. Lett. 88 (2006) 063105.
[8] K. Kawaguchi, M. Ekawa, A. Kuramata, T. Akiyama, H. Ebe, M. Sugawara, Y. Arakawa, Appl. Phys. Lett. 85 (2004) 4331.
[9] W.G. Jeong, P.D. Dapkus, U.H. Lee, J.S. Yim, D. Lee, B.T. Lee, Appl. Phys. Lett. 78 (2001) 1171.
[10] H.D. Kim, W.G. Jeong, J.H. Lee, J.S. Yim, D. Lee, R. Stevenson, P.D. Dapkus, J.W. Jang, S.H. Pyun, Appl. Phys. Lett. 87 (2005) 083110.

[11] P. Caroff, C. Paranthoen, C. Platz, O. Dehaese, H. Folliot, N. Bertru, C. Labbé, R. Piron, E. Homeyer, A. Le Corre, S. Loualiche, Appl. Phys. Lett. 87 (2005) 243107.
[12] H. Saito, K. Nishi, S. Sugou, Appl. Phys. Lett. 78 (2001) 267.
[13] Z.Y. Xu, Z.D. Lu, X.P. Yang, Z.L. Yuan, B.Z. Zheng, J.Z. Xu, W.K. Ge, Y. Wang, J. Wang, L.L. Chang, Phys. Rev. B 54 (1996) 11528.
[14] Q. Gong, R. Nötzel, P.J. van Veldhoven, T.J. Eijkemans, J.H. Wolter, Appl. Phys. Lett. 85 (2004) 1404.
[15] J.D. Lambkin, D.J. Dunstan, K.P. Homewood, L.K. Howard, M.T. Emeny, Appl. Phys. Lett. 57 (1990) 1986.
[16] F. Klopf, S. Deubert, J.P. Reithmaier, A. Forchel, Appl. Phys. Lett. 81 (2002) 217.
[17] H. Wang, D.T. Cassidy, IEEE J. Quantum Electron. 41 (2005) 532.
[18] R. Nötzel, N. Ledentsov, L. Däweritz, M. Hohenstein, K. Ploog, Phys. Rev. Lett. 67 (1991) 3812.
[19] R. Nötzel, J. Temmyo, T. Tamamura, Nature 369 (1994) 131.
[20] R. Nötzel, Z.C. Niu, M. Ramsteiner, H.P. Schönherr, A. Trampert, L. Däweritz, K.H. Ploog, Nature 392 (1998) 56.